Bioinspiration & Biomimetics

PAPER

Multi-legged steering and slipping with low DoF hexapod robots

Dan Zhao[1,3] and Shai Revzen[2]

[1] Department of Mechanical Engineering, University of Michigan, Ann Arbor, MI 48105, United States of America
[2] Department of Electrical Engineering and Computer Science, University of Michigan, Ann Arbor, MI 48105, United States of America
[3] Author to whom any correspondence should be addressed.

E-mail: danzhaoy@umich.edu and shrevzen@umich.edu

Keywords: multi-legged locomotion, hexapedal robots, steering, slipping

Supplementary material for this article is available online

RECEIVED
31 December 2019

REVISED
8 March 2020

ACCEPTED FOR PUBLICATION
30 March 2020

PUBLISHED
19 May 2020

Abstract

Thanks to their sprawled posture and multi-legged support, stability is not as hard to achieve for hexapedal robots as it is for bipeds and quadrupeds. A key engineering challenge with hexapods has been to produce insect-like agility and maneuverability, of which steering is an essential part. However, the mechanisms of multi-legged steering are not always clear, especially for robots with underactuated legs. Here we propose a formal definition of steering, and show why steering is difficult for robots with 6 or more underactuated legs. We show that for many of these robots, steering is impossible without slipping, and present experimental results which demonstrate the importance of allowing for slipping to occur intentionally when optimizing steering ability. Our results suggest that a non-holonomic multi-legged slipping model might be more appropriate than dynamic models for representing such robots, and that conventional non-slip contact models might miss significant parts of the performance envelope.

1. Introduction

Most animals and mobile robots move through the world by moving parts of their body to generate reaction forces from the environment and thereby propel themselves. Legged locomotion focuses on that subset of locomotion that employs intermittent contact forces generated by dedicated organs, the 'legs', for that propulsion. This is distinct from using fluid dynamic forces, as in fish swimming, or continous contact forces, as in wheeled vehicles. There are very few non-novelty commercial legged robots, and much of the focus in the field of legged robotics has been on bipedal or quarupedal robots. This is stark contrast to the natural world, where almost all animal groups that employ legs, employ six or more legs. Much of the objection to building robots with many legs has been the mechanical complexity of the associated device, which is directly tied to the number of degrees of freedom (DoF) in each legs (both actuated and unactuated).

In this paper we explore steering and slipping in hexpedal robots with legs with 1 or 2 DoF, i.e. legs whose point(s) of contact can only occupy a one- or two-dimensional manifold with respect to the body frame of reference. We draw attention to the importance and inherent difficulty of producing steering from such legs. We offer two contributions: (1) experimental results showing that slipping is highly beneficial for obtaining an increased steering range, suggesting that the practice of designing non-slip gaits misses an important part of the operational envelope of multi-legged robots; (2) evidence that despite slipping, in our hexapods the relationship between body frame motion and shape change appears to be 'geometric', i.e. computable knowing only shape and the rate of shape change, without knowing forces.

Below we provide some background (section 1.1), biological motivation (section 1.2), followed by theoretical preliminaries that precisely define the notion of steering as we use the term (section 1.3). We then discuss some of the impact of phase constraints on steering gaits (section 1.4), discuss steering strategies (section 1.5), and define the performance metrics we use to evaluate steering (section 1.6).

1.1. Previous work on multi-legged robots

The conventional approach to studying steering behavior in robots is to directly test proposed steering gaits on robot platforms and further explore the experimental results to explain and improve the achieved gaits. For fully actuated hexapod robots (active DoF per leg $d \geqslant 3$) inverse kinematics has been

used to plan footholds for precise quasi-static steering [Duan *et al* 2009, Shekhar Roy and Kumar Pratihar 2014]. However, multi-legged robots do not require fully articulated legs for dynamic stability. Even with 1 DoF or 2 DoF legs, hexapedal robots can still achieve stability and maneuverability—for example the RHex robot family [Galloway *et al* 2010, Saranli *et al* 2001] and the Sprawl robot family [Kim *et al* 2006, McClung 2006]. With all the actuators concentrated in the body, such low-DoF hexapod robots have lighter legs which can swing much faster than fully articulated legs, and further boost the speed of locomotion. They are also simpler to build and less complex to control compared with their fully articulated counterparts.

Several investigators have looked at maneuverability of hexapods: [McClung 2006] did a thorough investigation of the dynamic maneuverability of Sprawlettes (2 DoF per leg) and identified effective parameters that can be used for steering. Many interesting turning methods were also tested and studied on the RoACH family of rapidly-prototyped palm-size robots [Haldane and Ronald 2014, Pullin *et al* 2012, Zarrouk and Ronald 2015]. For OctoRoACH, [Pullin *et al* 2012] applied a differential speed method for dynamic turning by driving legs on different sides with a different frequency. Haldane and Ronald [Haldane and Ronald 2014] demonstrate that oscillations in height and roll angle determine VelociRoACH's turning behavior and developed a steering gait for VelociRoACH controlled by phase offset between the left and right sets of legs. 1STAR in [Zarrouk and Ronald, 2015] claimed to be the first steerable robot with only one actuator; it generated rotation by continuously accelerating and decelerating the legs resulting in the compliance disparity between alternate stance tripods. [Zarrouk *et al* 2015] also summarized the turning performance of these three palm-size robots and other famous multi-legged robots.

1.2. Maneuverability in biological hexapods

Unlike bipedal and most quadrupedal vertebrates, insects have legs sprawled outward in fore-aft and lateral directions, which offers them additional stability and exceptional maneuverability in horizontal plane, making them able to execute very tight turns at high speeds [McClung, 2006]. Even with similar sprawled structure, achieving such maneuverability in hexapedal robots is challenging. Getting better understanding of the steering behaviors is an essential part of improving planar maneuverability.

One approach is to study animal turning behavior and build models and hypothesis that would inspire robot design. Franklin *et al* [Franklin *et al* 1981] discovered two principal methods the cockroach *Blattella germanica* used to turn: increasing step frequency or step length of legs on one side of the body relative to the other, where the step length change was achieved by changing either the leg arc swing magnitude or functional length of the legs. Some extreme changes of step length like pivoting one leg in place or even moving one leg backwards were observed in bee turning by Zolotov *et al* [Zolotov *et al* 1975]. Jindrich and Full [Jindrich and Full 1999] measured the full dynamics of turning in the cockroach *Blaberus discoidalis* and analyzed the contributions of each leg to turning, concluding that turning dynamics can be characterized as a minor modification of straight-ahead running. To describe motion of cockroaches in the horizontal plane, several models were developed by Proctor and Holmes [Proctor and Holmes 2008]; Schmitt and Holmes [Schmitt and Holmes 2000]; Seipel *et al* [Seipel *et al* 2004]. Our own study of running *B. discoidalis* cockroaches [Sachdeva *et al* 2018] observed that a large fraction of cockroach foot motions are 'slipping' in the sense that the feet are moving with respect to the ground while in contact with it as shown in figure 1. It seems that the cockroaches exhibit far less non-slip ground contact than assumed in published locomotion models.

1.3. Definition of steering with a periodic gait

Legged systems (animals and robots both) typically move using a *periodic gait*[4]: a cyclic shape-change which produces (at least on average) a motion through the world. The shape-change can be represented by the leg motions in the body frame of the system. Thus, each leg is repeating the same motions every period of a periodic gait, and the body is thereby propelled in a similar way each cycle.

For moving on a horizontal plane, we typically desire robots to allow us to control position and heading. We will refer (by slight abuse of terminology) to the rigid body motion generated (at least on average) by a single period of a periodic gait as the *holonomy* of that gait. The framework of geometric mechanics provides a precise language for describing how holonomies arise from periodic shape changes [Bloch *et al* 2005, Marsden and Ostrowski 1998]. The partitioning of system configuration into body frame and (body) shape is so intuitive that most of the time we assume its validity without careful examination, however, as a technical point, we note that geometric mechanics shows that when the mechanics of a system are governed by a Lagrangian symmetric under the Lie group SE(2), i.e. when the mechanics are the same in all positions and orientations on a plane, the symmetry always induces a principal fiber-bundle structure allowing a configuration q of the system to be represented in terms of a *body frame*[5] pose g in the world, and a *shape* b of the robot.

[4] Some authors conflate the term 'gait" with 'periodic gait'; the definition and discussion of non-periodic gaits is outside the scope of this manuscript.

[5] Although this may seem to childishly obvious, defining a body frame for e.g. a slithering snake, is non-trivial and has significant computational implications [Hatton and Choset, 2011].

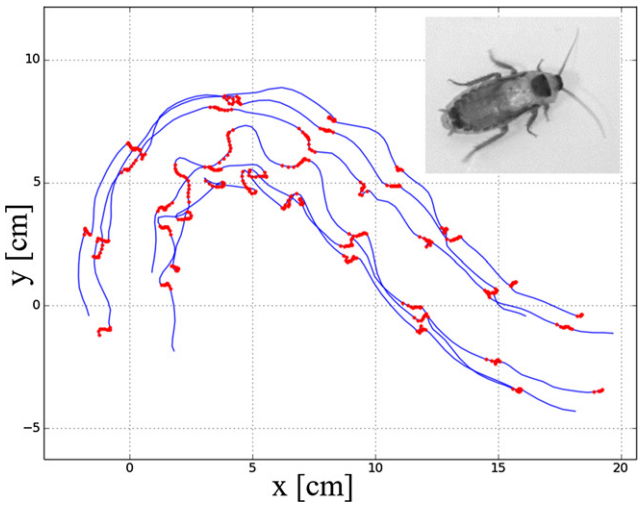

Figure 1. Cockroaches slip while running. We recorded 24 trials of *B. discoidalis* running at 15–77 cm s^{-1} on foamcore [Elmer's 900803 Foam Board]. Averaged by trial, front, middle, and hind legs slipped 18%, 15%, 16% of their total travel distance. We show the tarsus (foot) trajectories recorded in the world frame while moving forward relative to the body (blue), and while moving backward (red). Note: synchronized side-view videos suggest that feet moving back with respect to the body are in contact with the ground.

The instantaneous configuration $q = (g, b)$ is an element in the overall configuration space $Q = G \times B$. The shape space B is typically a compact manifold in $\mathbb{R}^k$ for some $k > 1$, and represents the possible shapes of the body, with the current shape being $b \in B$. The instantaneous body frame $g \in G$ is an element of the group G, which for horizonal motions is the group of rigid body motions in the plane, SE(2).

Executing a cyclic shape change does not, in general, correspond with a cycle in body frames. While the shape starts and ends the same over a cycle, the body frame changes, constituting motion.

Consider a system moving using a periodic gait with period T, and configuration given by $(b(t), g(t)) \in B \times G$. The body shape $b(t)$ must also be periodic with period T. The holonomy of this gait would be $\Delta g := g(t+T)(g(t))^{-1}$, and is the same for all choices of t. The theory of geometric mechanics tells us that $g(t)$ is completely defined by knowing $g(0)$, $\dot{g}(0)$ and $b(t)$. To capture the fact that the gait is defined by a *periodic* $b(t)$ we will take the domain of $b(\cdot)$ to be the unit circle $\mathsf{S}^1 \subset \mathbb{C}$. Instead of thinking of $b(\cdot)$ as a function of t, we shall take $b(\varphi)$, $\varphi \in \mathrm{S}^1$, and $\varphi(t) = \exp(i2\pi t/T)$.

A holonomy in our case is a rigid body motion and can be represented in homogenous coordinates (see equation (1)), where $\Delta\theta$ is the orientation change; and Δx and Δy are the translation of body frame origin as shown in figure 2.

$$\Delta g = \begin{bmatrix} \cos(\Delta\theta) & -\sin(\Delta\theta) & \Delta x \\ \sin(\Delta\theta) & \cos(\Delta\theta) & \Delta y \\ 0 & 0 & 1 \end{bmatrix} \qquad (1)$$

We define *steering* to be the ability to select the rotational component $\Delta\theta$ of the holonomy Δg within an interval around 0 by employing a one-parameter family of periodic gaits. Thus, a steering gait is a function:$b(\varphi, s) : \mathrm{S}^1 \times [-\theta_m, \theta_m] \to B$, such that the holonomy $\Delta g(s)$ for the gait $b(\cdot, s)$ has a rotational part $\Delta\theta$ equal to s. We further require that the map $\Delta g(s)$ be continuous in s, i.e. small changes in steering parameter lead to small changes in the resulting holonomy. The astute reader may note that we have omitted the discussion of T and its potential dependence on s. For now, we will assume that a steering gait has a common period T used for all choices s. However, it should be noted that if the motion is in practice 'geometric', as we will later claim, the holonomy is in fact independent of the choice of T, making this issue moot.

Steering and turning are two terms we often see used in describing locomotion. We use the terms 'steer' and 'turn' to refer to different phenomena: turning is the rotational component of the body frame; steering is the ability to do so continuously with magnitudes of turn in an interval containing 0 (pure translation) while at the same time also translating. Thus, one can 'turn in place', but not 'steer in place'. More interestingly, a robot might have some acheivable discrete translation–rotation motions available, i.e. the ability to 'move and turn', without the ability to steer. This can happen, for example, by doing two full steps on one side of the body, while taking one full step on the other side.

1.4. Phase constraints limit periodic gaits

It should be noted that repeated motions of individual legs do not, on their own, make a periodic gait. To be periodic, the motion of all legs together must be periodic. Thus, if one considers each leg as an independent subsystem executing a periodic

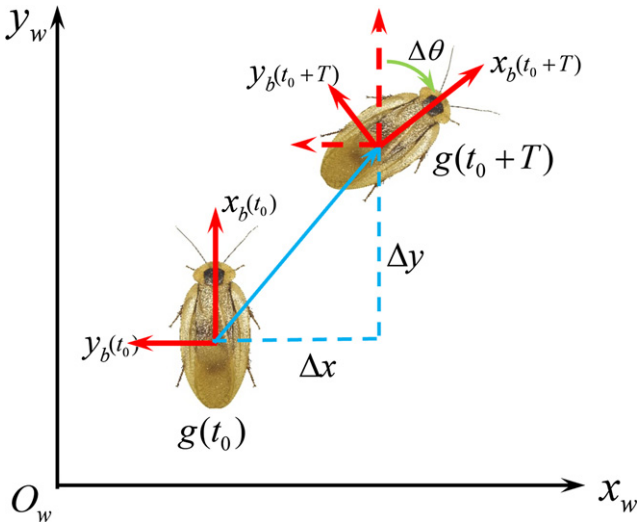

Figure 2. Coordinate frames for definition of steering.

motion, the periodicity of body motion implies a constant phase difference constraint between the 'sub-system phases' [Revzen *et al* 2008] of the respective legs.

To illustrate why this phase constraint has important implications, let us compare a legged system to a typical wheeled vehicle with wheels on both sides of an axle. When the vehicle turns by an angle, the left and right wheels incur a permanent phase shift representing the difference between the arc lengths traveled by the two sides. It is for this reason that wheeled vehicles have a 'differential' in their axle. Because the wheels are symmetric under their axis of rotation, they are symmetric under phase change, and this phase shift is of no consequence for future motions; to the best of our knowledge its only use is the chalk marks made for parking enforcement, which use this phase difference to detect if a car has moved.

In legged systems, such shifts could produce significant changes in motion. For example, the difference between trotting, pronking, and pacing in quadruped gaits is primarily having a different, yet constant, difference between the sub-system phases of the legs [Wilshin *et al* 2017]. Not only do different gaits have corresponding phase constraints, there typically are phase differences that do not generate viable gaits. For example, there can be phase differences which place no leg to support the body over a period of time, resulting in the robot body falling on the ground. To support the body, legs of a multi-legged robot must maintain their phase differences within a limited viable range. For example, many hexapods can maintain quasi-static balance by ensuring that at all times there is a set of legs contacting the ground at points which surround the horizontal projection of the center of mass (COM)—a constraint that can be formulated in terms of phase locking.

1.5. The geometry of steering strategies

Each periodic gait $b(\cdot, s)$ embeds the circle S^1 in the shape space B. Thus $b(\cdot, s)$ is described entirely in terms of a geometric object—its image in B, comprising a one-dimensional collection of body shapes (see figure 3(a))—and the rate at which these shapes are adopted. In those cases where the physics create a 'principal kinematic system', that rate information has no bearing on the resulting holonomy, and the gait can be thought of as a purely geometric entity—a loop in shape space. Changing holonomy to steer must therefore require changing this loop (e.g. to figure 3(b)).

1.5.1. Changing timing to steer

Consider the case of a robot with 1-DoF legs. Each leg is mechanically constrained to a fixed one-dimensional track; the only change available to such a leg is changing its timing, e.g. changing the duration it spends moving slowly vs moving quickly in a given cycle (figures 3(c) and (d)). Even though the shape of the physical motion of each leg cannot change, and only its rate moving along its cycle can be modulated, this is not equivalent to being restricted to merely changing the rate of a fixed gait. The key difference is that when changing the rate of a gait, all legs change rate precisely the same way together. Even with 1-DoF legs, when the rates of individual legs along their cycles is modulated differently in different legs, the resulting shape-space loop is *geometrically* different (figure 3(b)). However, because of the phase constraints (see section 1.4) that need to be maintained, the rate modulation of individual legs must integrate to an integer number of cycles after a period. Typically, that integral will be 0, implying that all legs executed the same number of steps. While some legs can be 'sped up' relative to other legs, they must then also

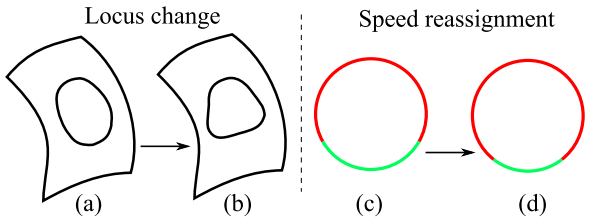

Figure 3. Illustration of gaits and gait change. Gaits occupy a loop in shape space (a) since they are an image of the circle S^1. To modulate a gait we may change that image in shape space (b). Alternatively, viewing each leg's motion as a cycle [(c) and (d)] with fast (red) and slow (green) segments, a gait can be modulated by changing which parts of the cycle are executed at which speed [(c) vs (d)] for each individual leg.

be 'slowed down' to resynchronize the legs at the end of the cycle.

1.5.2. The special case of bilateral symmetry in the plane

Consider a system (animal or robot) which is bilaterally symmetric. This implies the existence of a symmetry map $S : B \to B$ and an associated $\hat{S} : \mathfrak{se}(2) \to \mathfrak{se}(2)$ which map body shape to its mirror image, and body velocities to their mirror images. Both of these maps must be involutions, i.e. $S(S(b)) = b$ and $\hat{S}^2 = I$. Furthermore, in the case of planar motion in particular, regardless of the choice of body symmetry axis, the operator $\hat{S}$ flips the sign on rotational velocities.

It is quite common for bilaterally symmetric organisms to employ 'symmetric gaits' for translation, i.e. $S(b(\varphi, 0)) = b(-\varphi, 0)$ (note: $-\varphi = \exp(i\pi)\varphi$, the phase after a half-cycle). In such gaits the cycle of body motions consists of two mirror image halves; the first half cycle is the mirror image of the second half cycle.

The associated body frame velocities $g^{-1}\dot{g}$ satisfy $\hat{S} \cdot g^{-1}(\varphi)\dot{g}(\varphi) = g^{-1}(-\varphi)\dot{g}(-\varphi)$, i.e. they too are mirrored after half a cycle, and therefore the rotational velocities too are mirrored. In both 3D and 2D, the rotational part of motion is unaffected by translation, i.e. one can compute the total rotation of a sequence of rigid body motions without knowing the translation. This corresponds to the algebraic property of both groups being semidirect products $\mathsf{SE}(3) = \mathsf{SO}(3) \ltimes (\mathbb{R}^3, +)$ and $\mathsf{SE}(2) = \mathsf{SO}(2) \ltimes (\mathbb{R}^2, +)$. In the special case of 2D, $\mathsf{SO}(2)$ is commutative, and therefore the rotations occurring in the second half of the gait cycle perfectly cancel those occurring in the first half, leading to a pure translation.

Thus it is a special feature of 2D planar motion (and of 2D planar motion only!) that symmetric gaits always produce a net translation with no rotation. Many organisms and robot designers employ this feature to produce translation from legged systems[6].

[6] The naive reader might assume that the translation created by a symmetric gait must be along the axis of symmetry; this is untrue. Rather, the set of translation directions acheivable is itself symmetric; every gait that lists to left has a partner that lists to the right by the same angle.

It further follows that by introducing a parametric change in one half of the cycle, one is likely to introduce a net rotation, and that by introducing the self-same parametric change in the other half cycle containing the mirrored portion of the motion, one may introduce a rotation of the same magnitude but opposite sign. Then in-cycle modulation of such parametric asymmetry makes the original symmetric gait a steering gait.

As humans it is hard for us to conceive of any other way to produce translational motion and to modulate it by steering, since bilateral symmetry is so ingrained in our morphology. Still, we must exercise caution in assuming all legged systems must use this approach. For example, horses use a 'rotary gallop' gait which is not bilaterally symmetric when moving at high speeds; therefore they are likely to use non-mirror strategies for steering left and steering right.

1.6. Performance criteria for steering

Existing literature suggests different performance metrics for quantifying steering. [McClung 2006] suggest the metric of $v\dot{\theta}$ that combines the angular turning rate $\dot{\theta}$ with forward speed v. This metric is dimensional, and gives a natural advantage to high-speed running robots with dynamic steering gaits. Zarrouk *et al* [Zarrouk *et al* 2015] used the metric of average heading change per step, which is estimated from the average turning rate and the step rate, to summarize the turning performance of a dozen of famous multi-legged robot platforms. We will use a similar metric—the turning angle per cycle in (deg/cyc)—and also use a geometric measure of turning: the turning radius in (mm).

Compared with the metric of turning angle per step in Zarrouk *et al* [Zarrouk *et al* 2015], turning angle per gait cycle can be applied to more cases, as the notion of 'step' is only meaningful in symmetric gaits. Typically in steering the two steps in one gait cycle have noticeably different turning angle, making turning angle per step bimodally distributed.

Turning radius is a world-frame measure which represents how sharp a turn the steering gait can achieve, and is thus an important parameter for motion planning.

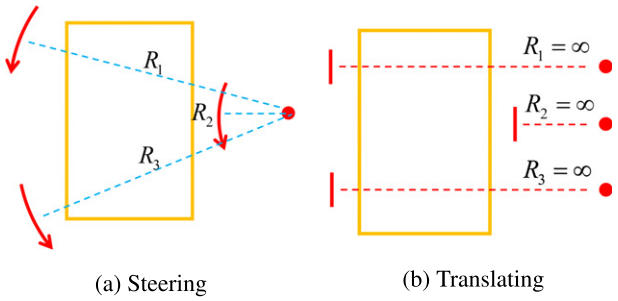

Figure 4. Leg strokes in the body frame for a tripod of legs, assuming non-slip motion while steering (a) and while translating without heading change (b). Note that leg strokes needed for non-slip steering and noslip translation have incompatible 2D projections in the body frame, and thus cannot be the result of the same 1-DoF motion.

2. Multi-legged steering with low DoF legs

From this section on we restrict our attention to multi-legged systems which have sufficient friction with the ground to justify the claim that COM momentum (known as 'group momentum' in geometric mechanics) dissipates quickly[7]. Typically, this would be the consequence of having 3 or more point contacts with the environment at all times; if contacts can support torques, fewer contacts than 3 might suffice. Our assumption rules out discussion of highly dynamic gaits with low duty cycles, and the gaits of bipeds, and the more rapid gaits of quadrupeds.

We will discuss legs with 1 or 2 DoF, where by DoF we only include active DoF-s that can be directly controlled. Passive DoF, like the deformations of elastic legs, are not included. In this, the issues facing low-DoF multi-legged robots are the converse of those facing the typical bipedal or quadrupedal robot: the former are over-constrained with respect to the ground, whereas the latter are under-constrained.

2.1. Steering with these conditions is hard

To futher illustrate the importance of the investigation we conducted, consider the conditions for multi-legged low DoF steering. Removing any one component of 'multi + legged + low DoF + steering' produces an easier to solve problem.

If 'legged' is not a requirement: many wheeled vehicle have low DoF multi-contacts with ground, but such contacts are continuous. The continuous symmetry of the wheels allows them to have arbitrarily accumulated phase from the phase difference introduced with steering. This implies that wheeled vehicles switch within an $N-1$ dimensional family of functionally identical periodic gaits (N number of wheels), one for each possible choice of phase differences between the wheels. In that sense, wheels or treads solve a different, far easier problem.

[7] By 'quickly' we mean that we are in the domain where the recent results of [Kvalheim *et al* 2019] apply, implying that the equations of motion can be written in an approximately geometric form (ibid).

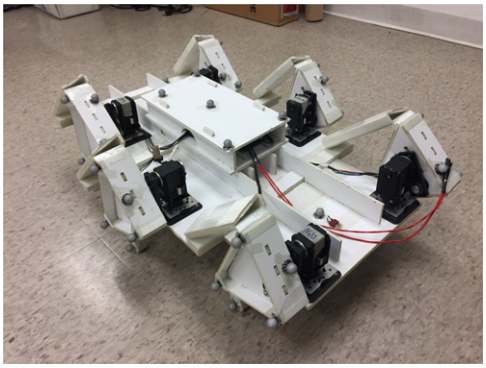

Figure 5. BigAnt.

If 'multi-' is not a requirement: for bipedal robots with low DoF legs, only one leg is touching the ground for most of the time. Bipedalism creates substantial problems in controlling an under-actuated, unstable plant. For bipedal robots, the bigger challenge is to maintain heading and stability—a single pin-joint contact, or even a toe and heel pair of contacts, often generate heading and orientation changes that can be exploited for steering. It should also be mentioned that with only two legs, 3 DoF per leg requires only 6 motors, i.e. a device of comparable mechanical and electrical complexity to a hexapod with low DoF legs.

If 'low-DoF' is not a requirement: as soon as each leg has 3 or more DoF, foot placement can be arbitrarily controlled within a volume, making the body frame fully locally controllable in a kinematic sense. At the cost of this extra complexity, steering becomes much easier, at least at the low speeds we consider here.

It is also important to notice that these conditions do not make locomotion uniformly difficult; we have only identified these difficulties in the case of steering. If the robot is not required to allow the heading to be continuously controlled while moving, making the robot bilaterally symmetric allows one to exploit the trick described in section 1.5.2 to translate without rotation. In particular, in the case of hexapod

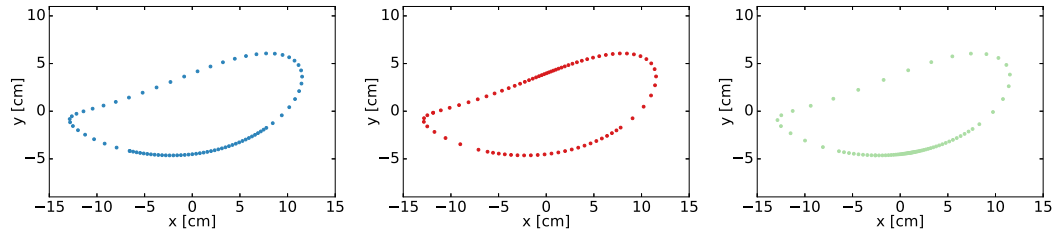

(a) No steering (b) ML, $s = 0.55$ (c) MR, $s = 0.55$

Figure 6. Leg trajectory in the body frame, with points indicated at equal phase intervals. Without steering (a) a clear Buehler clock effect is visible. With steering at $s = 0.55$, the timing of ML (b) and MR (c) becomes different, even though the shape of the trajectory is the same.

robots, a designer may use the alternating tripod gait. In such a gait, the three feet in contact with the ground form a triangle under the center-of-mass and translate relative to the body without changing the shape of the triangle. This uniquely defines the motion of the body frame, and given bilateral symmetry, allows for a walking gait with zero heading change.

From these examples, we can see that multi-legged steering with low-DoF legs is particularly hard to understand. Solving this problem would allow us to better use multi-legged robots with a mechanical and electrical complexity lower than that of today's popular bipeds and quadrupeds.

2.2. 1-DoF steering creates conflicting constraints

To be able to translate using a set of non-slip foot contacts, those foot contacts must themselves translate as a rigid set of points in the body frame while in stance. This geometric constraint must be designed into the motion of any set of legs used for non-slip motion. Note that this geometric constraint is necessary, but not sufficient to make a gait have no slip: accelerations or gravitational force components can be large enough to break a contact outside its friction cone and cause it to slip anyway. The gaits we describe are slow enough, and stable enough where all slipping is caused by incompatible foot motions.

The problem of incompatible foot motions becomes starkly clear when considering a robot with 1-DoF legs (see figure 4). The feet of 1-DoF legs follow a one-dimensional path in the body frame. Whichever feet support the body while translating (we assume a tripod in figure 4), they must follow identical paths in the body frame. Whichever feet support the body while steering along some arc, the feet must follow different paths from each other for non-slip contact because they are at different radii from the center of rotation. Since the legs are assumed 1-DoF, each individual leg can only follow one path—showing that allowing a range of turning radii creates conflicting constraints on the 1-DoF path of the feet.

Naively, one might assume that hexapedal robots with 1-DoF legs moving parallel to the body would have trouble steering and turning. In practice, direction changes merely force the robots break the non-slip constraint. For example, RHex is highly maneuverable [Johnson 2013] and turns easily, but it does so with considerable slipping.

3. Results: low-DoF hexapods steer with slipping

To verify our analysis about low-DoF multi-legged steering and measure slipping behavior during steering, we used two types of robot platforms that have different morphology and different effective DoF per leg (1-DoF and 2-DoF) for our experiments. We tested both robots on two substrates—a relatively slippery linoleum floor, and higher friction interlocking rubber tiles (C9 interlocking fitness mat; Target Inc 2015). We tried a variety of steering parameters and speeds. All the locomotion results were recorded using a reflective marker motion tracking system (10 Qualisys Oqus-310+ cameras at 120 fps, running QTM 2.17 build 4000, interfaced to custom SciPy 0.17.0 code using the Qualisys 1.9 Realtime API)

3.1. BigAnt 1-DoF hexapedal robot

Our 1-DoF robot tests were conducted on the BigAnt robot. The design and development of BigAnt is outside the scope of this paper, and only summarized briefly here. Its chassis structure and mechanisms were manufactured using the PARF (plate and reinforced flexure) technique [Fitzner *et al* 2017, Miller *et al* 2015] developed in our lab. Using PARF, the chassis of BigAnt can be manufactured with minimal tooling (a knife) and less than US$20 worth of materials (Elmer's Products Inc. foam board 508 × 762 × 7mm and 3M Scotch #8959 fiber tape). With a laser cutter instead of the knife, the chassis can be fabricated within 7 h, which includes 30 min assembly. The fast and inexpensive turnaround allowed the design of BigAnt to be iterated quickly. Instead of simulating each re-design we used experiments to directly measure and iteratively improve the robot (see figure 5 for version used here).

Like the RHex family of robots [Galloway *et al* 2010, Saranli *et al* 2001], BigAnt has six 1-DOF legs. Each leg is actuated by a servo motor (Robotis Dynamixel MX64), but rather than directly rotating a

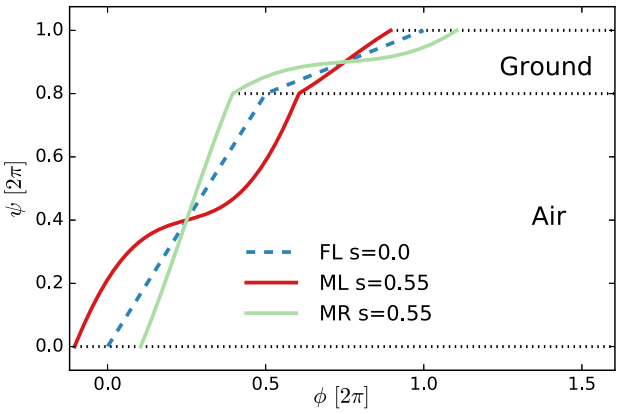

Figure 7. BigAnt joint angle output as a function of local phase φ within a gait cycle. When moving straight, the phase to joint angle relationship is a 'Buehler clock' consisting of a fast constant speed phase for aerial motion and a slow constant speed phase during expected ground contact (dashed blue line). With a steering input of $s = 0.55$ (see equation (2)), the mid left leg motion (red) and mid right leg motion (green) are modulated in opposite ways, generating a steering motion to the right.

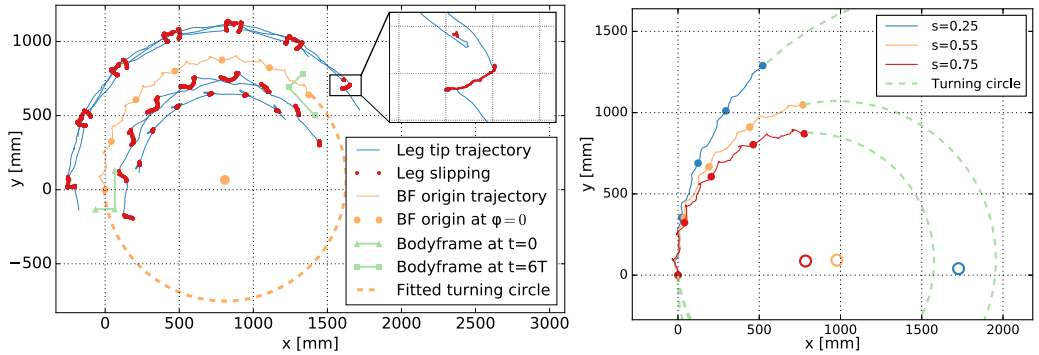

Figure 8. BigAnt motion in world frame (left) and steering results at different values of s (right). For gait frequency $f = 0.22$ Hz; steering input $s = 0.75$, we plotted (left) leg tip trajectories (blue), with slipping highlighted (red dots; magnified in inset), and the trajectory of the body frame origin O (yellow line) with the beginning of cycle indicated (yellow dots). We indicated the markers that define the body frame (light green) at the beginning (triangles) and end (squares) of this 6 stride trial. To estimate turning radius we fit a circular arc (dotted yellow) to the body frame origin. In this trial, BigAnt turns 23 deg/cyc and the turning radius is 818mm. Exploring other values of s (right) we plotted the motion of the body frame origin at different values of the steering parameter s (teal, yellow, red for 0.25, 0.55, 0.75 resp.), while leaving all other gait parameters unchanged. To each trial of 4 strides we fitted a circular arc (dashed green) and indicated the center of rotation (teal, yellow, red circles). Results suggest a clear parametric dependence of turning radius on steering parameter value. See supplementary videos (available at stacks.iop.org/BB/15/045001/mmedia) for illustrative examples.

leg like RHex robots do, the legs of BigAnt are driven through a 4-bar mechanism. The leg trajectory was chosen by exploring the space of possible 4-bar designs for motions with a flattened backward stroke and a high clearance when swinging forward (see figure 6(a)). While other linkages exist that could produce a flatter back stroke, those require significant additional complexity or larger dimensions compared with the current 4-bar design. The BigAnt leg is highly modularized, making it easy to both replace worn out legs, and install custom leg geometries for different applications.

3.1.1. BigAnt steering gaits

While the 4-bar linkage defines the geometry and position-dependent gearing ratio of BigAnt legs, the instantaneous position of the leg along its ovoid path is under (conventional PID based) servo control. If all six legs are driven at constant angular speed as two anti-phase tripods of legs ('left tripod' FL-MR-HL containing [F]ront-[L]eft, [M]iddle-[R]ight and [H]ind-[L]eft legs; and the 'right tripod' FR–ML–HR), the robot exhibits substantial up-down motions representing parasitic work against gravity. To obtain a smoother motion, we scheduled the motion of the shaft angles $\psi_k, k \in \{\text{FL, FR, ML, MR, HL, HR}\}$ as a function of leg phase φ_k using a two-speed schedule: a (typically) fast 'aerial phase', and a (typically) slow 'ground contact phase' (see figure 7). To our knowledge, this idea comes from work done by M. Buehler on the RHex robot, and is sometimes referred to as a 'Buehler clock' in the RHex literature. The Buehler clock is defined by 4 parameters. Often these are the 'sweep' angle through which the leg moves in ground contact, a 'duty cycle' defining the fraction of the cycle in ground contact, the stance angle 'offset' away from vertical, and the phase at midstance. Because the choice of zero phase is

Table 1. Slipping by leg for $s = 0.75$, $f = 0.22$ Hz. Motion capture error bounds were ± 3.5 mm at 99th percentile of error.

	FL	ML	HL	FR	MR	HR	Mean
Slip/cyc (mm)	98	48	119	115	60	133	95
Slip ratio (%)	18.7	9.6	22.1	28.7	13.8	30.9	20.6
Abs. tangent (mm/cyc)	45	40	66	97	52	96	66
Abs. radial (mm/cyc)	79	18	81	49	20	77	54
Avg. tangent (mm/cyc)	−9	26	31	25	−5	35	17
Avg. radial (mm/cyc)	−47	5	44	−12	2	38	5

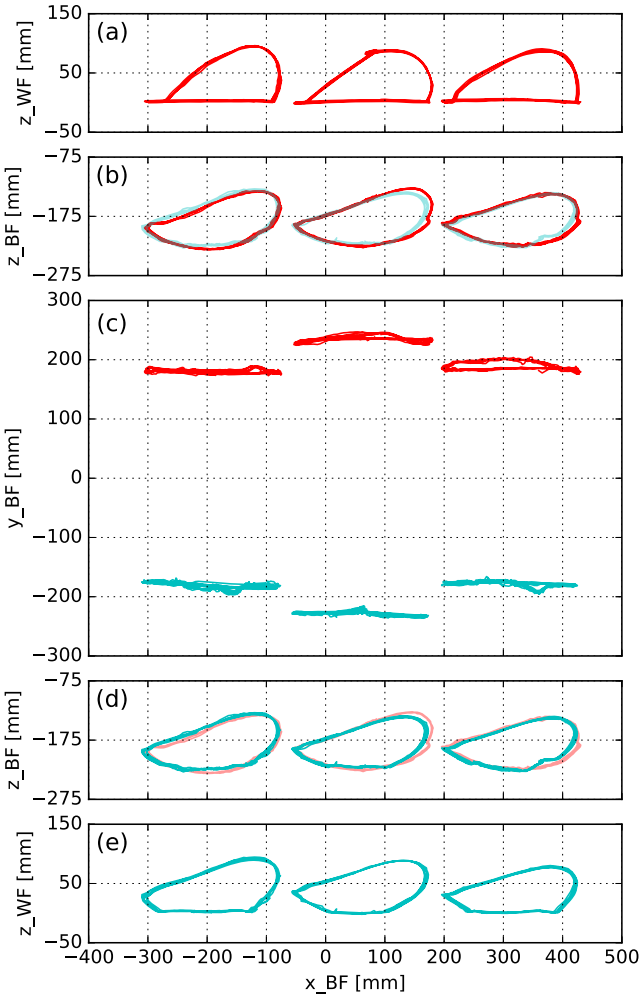

Figure 9. BigAnt foot motion in the body and wold frames. We show horizontal (x, y) projection (c) and saggital (x, z) projections (a), (b), (d), (e) with side of the leg indicated by color (left—red; right—teal). In the body frame (b), (d), the contralateral leg is also shown (transparent) to highlight that motions are symmetric in the body frame. Viewed with world frame z (0 is ground), the left legs (a) have a longer ground stroke than the right legs (e). This highlights the counter-intuitive notion that actual ground strokes can be quite different even with identically shaped trajectories, thanks to timing and slipping.

arbitrary, we always chose the liftoff phase to be 0, leading to a Buehler clock defined by only 3 parameters.

We designed our gaits by tweaking these three gait parameters at a moderate gait frequency (~ 0.2Hz) until the robot was both moving reliably and hardly bouncing up and down. We then introduced steering control by modulating the functions ψ_{ML} and ψ_{MR} with a steering input s. The overall phase change of such a modulation must be 0; it is therefore a periodic function of phase. We chose an obvious candidate—$\cos(2\pi\varphi)$ which we used to advance/retard the phase of one middle leg, and retard/advance the phase of the other middle leg in an anti-symmetric way. Letting $b(\varphi) : \varphi \mapsto \psi$ be the Buehler clock function chosen, our shaft angles were:

$$\begin{aligned} \psi_{\mathrm{FL}} &= \psi_{\mathrm{HL}} := b(\varphi) \\ \psi_{\mathrm{FR}} &= \psi_{\mathrm{HR}} := b(\varphi + 1/2) \\ \psi_{\mathrm{ML}} &:= b(1/2 + \varphi + s\,k_s\,\cos(2\pi\,\varphi)) \\ \psi_{\mathrm{MR}} &:= b(\varphi - s\,k_s\,\cos(2\pi\,\varphi)) \end{aligned} \tag{2}$$

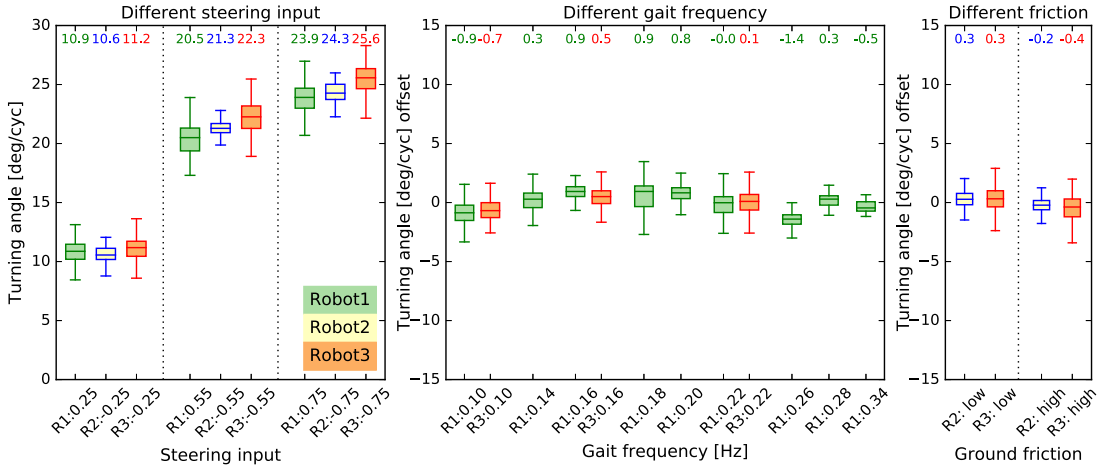

Figure 10. Turning rate dependencies on various parameters. To show dependence (or lack thereof) of turning rate on various parameters, we binned data according to the parameter value and collected a bootstrap sample of size 1000, making the spread of the various box-plots meaningful for comparison. We also present the numerical mean values of each box plot (number above box-plot). First, we group data by which of the 3 comparable robots (R1, R2, R3; green, yellow with blue frame, orange) we took data from, and at what value of the steering parameter s that trial was running (0.25, 0.55, 0.75 parts of the left sub-plot). Results show a clear dependence of turning rate ω on s, which is consistent among all 3 robots. Since the influence of s and robot ID r dominated variability in ω, we subtracted the average $\langle\omega\rangle(s, r)$ from ω to examine the data for any additional effects of gait frequency (0.10 Hz to 0.34 Hz middle subplot), or ground-to-foot friction coefficient (right subplot). Results fail to reject the null for these potential influences. Together, these results suggest that s alone governs the turning rate for each robot, and does so reliably for all the robots of this type we built.

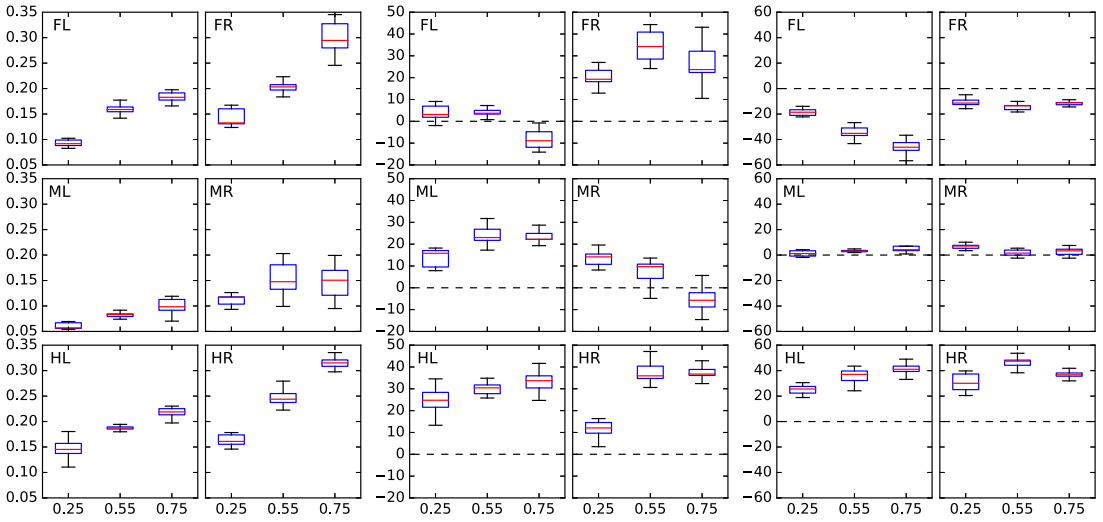

(a) Slip ratio (b) Average slip, tangent [mm] (c) Average slip, radial [mm]

Figure 11. BigAnt slipping metrics, by leg and steering parameter value. We collected the slipping metrics for BigAnt platform R1 with $f = 0.22$ Hz, partitioned by $s = 0.25$, 0.55, and 0.75. We present the ratio of slipping distance to travel distance (a); average distance slipped tangent to direction of motion along the turning arc (b); and average distance slipped radial to turning arc and thus perpendicular to direction of motion (c). Slipping in (b) is non-productive for locomotion; slipping in (c) is necessary to rotate the robot around its axis. Each metric is presented separately for each of the robot's legs. We created each box-plot by evaluating the metric by a bootstrap sample of 100 period-long windows from the relevant slice of the dataset. Note that with this gait the robot arcs to the right.

where $k_s := 0.24$ is a constant gain adjusting sensitivity. The shaft angles with steering modulation of $s = 0.55$ are shown in figure 7. The corresponding leg trajectories at figures 6(b) and (c) give us an explicit view of how the mid right leg is slowed down at ground contact and how the mid left leg is sped up at the same part of trajectory. With such modulated tripod gait, we can now steer BigAnt by changing the input parameter s to different values.

The strategy of steering by modulating middle legs is itself bio-inspired, and based on the strategies cockroaches often use for turning [Jindrich and Full 1999].

3.1.2. BigAnt steering gait test results

We tested the steering gait introduced in the previous subsection on BigAnt with different steering input parameters and recorded the motion using Qualysis

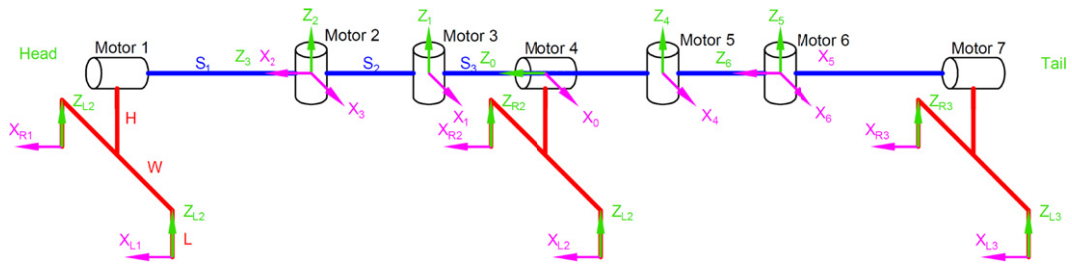

Figure 12. Mechapod is actuated by 7 highly geared down servo motors (Dynamixel MX106 and MX64): 4 of them are on the spine controlling the spine yaw motion (motor 2, 3, 5, 6); the other 3 controls leg roll motion (motor 1, 4, 7). The 3 pairs of legs are coupled by spring steels which offer compliance to the robot.

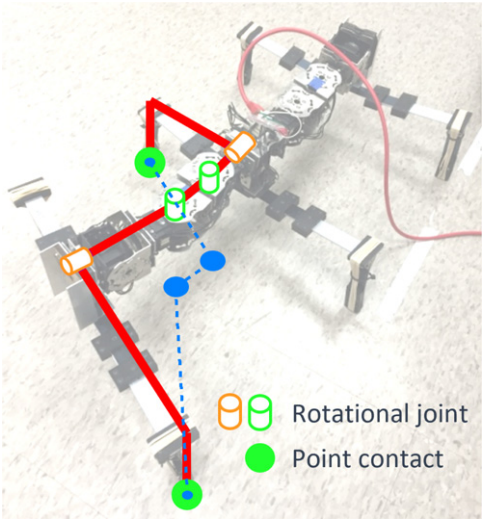

Figure 13. Overlay showing how Mechapod contains a 4-bar linkage. When the roll motors (orange cylinders) are activated and holding stationary at equal angles, the robot can be standing on a tripod (here FL, MR, HL) with presumed point contacts at the feet (green dots for FL, MR). The projection of the robot on the horizontal is then a 4-bar linkage (blue dots and dashed lines).

motion capture systems. Figure 8 shows an example of BigAnt walking on our lab floor; we provide detailed plots and statistics for this trial which consisted of 6 strides at gait frequency $f = 0.22$ Hz and steering input $s = 0.75$. Results from other trials were quite similar, and so we do not provide such details from every trial. We collected a total of $N = 39$ trials, $N_s = 225$ strides, total time of $\sim$ 1800 s at 120 fps for a total of $N_f = 2.16 \times 10^5$ frames of data, using $N_r = 3$ similarly constructed robots.

Additionally, we collected various metrics of slipping: (1) the slipping distance; (2) the 'slipping ratio' of slipping distance to total leg motion distance. A slipping ratio of 0 indicates a non-slip gait; a slipping ratio of 100% represents a leg that always remains in contact with the ground and is never in static friction. The average slipping ratio for the trial (figure 8) we examined in details is 20.6%. To better understand the kind of slipping taking place, we separate slip into two components: slipping in the direction tangent to the arc the robot is moving along, and slipping in the direction radial relative to this arc. For the slip in each components, we compute both the time-averaged absolute value, and the time-averaged value (see table 1).

We also examined the foot motions with respect to the body frame. Our expectation was that foot motions are, for all practical purposes, rigidly dictated. Therefore, regardless of the value of s or which of the 6 identical (up to mirror image) legs we observe, we should see the same trajectory for the foot in the body frame (see figures 9(b)–(d)).

To get more details about how the interaction between leg and ground results in such steering behavior, we plotted world frame z motion vs body frame x (see figures 9(a) and (e)). These two subfigures show a longer stroke in ground contact for all left legs, compatible with the observation that the robot turned to the right.

3.1.3. BigAnt turning rate results and slipping results

At this point it should become quite clear that while BigAnt is not hard to steer with our choice of steering gait (see figure 8 for steering with different inputs of s), the actual mechanical interaction that produces steering from the modulation of ψ_{ML} and ψ_{MR} with s is not at all obvious.

To better understand how BigAnt actually steers we conducted a multi-robot, multi-parameter study, summarized in figure 10. We compared the results taken from 3 independently constructed copies of the BigAnt robot, over a variety of gait frequencies, and on both low friction and high friction substrates. The purpose of this comparison was to establish whether it was in fact s which controlled the steering behaviors, or whether we merely created systems whose multi-contact interaction too complex for us to understand in some idiosyncratic way.

Since the experimental datasets are of slightly different sizes, and there is no reason to assume the parameters we measure are normally distributed, we used non-parametric methods for our statistical analysis. Each grouping of parameters was represented by a bootstrap sample of size 1000; this size was chosen because all groupings were at least of this size.

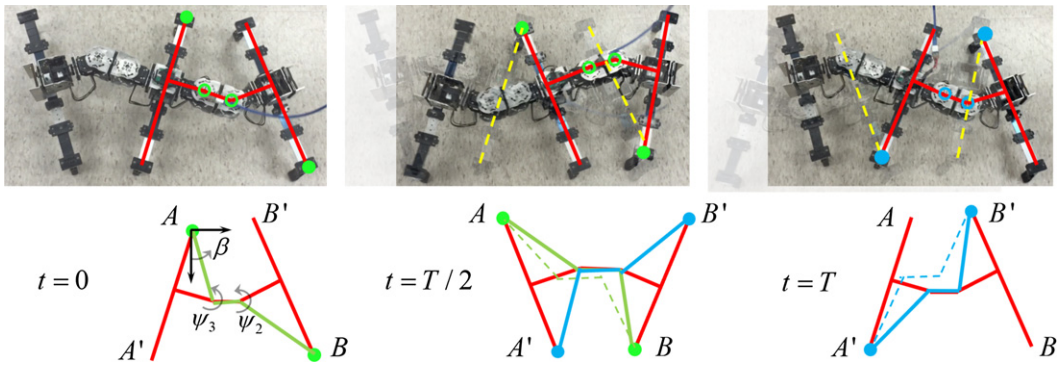

Figure 14. Mechapod locomotion can be represented by the motion of two 4-bar linkages. We show 2 consecutive steps of Mechapod walking left to right (top row; 3 photos of double stance configuration). We indicate the skeleton of the front half (red lines; open circles for motors) and the previous leg positions (dashed yellow). Supporting legs in first step (solid green circles) and in second step (solid blue circles) show the pivots of the abstracted 4-bar (bottom row). The first step 4-bar (green) and the second step 4-bar (blue) share link lengths and there is a well defined relationship between the angles of the links before and after the support switch for a fixed value of spine motor angles ψ_2, ψ_3. We denote the locations of the feet by A, B, A', B', and by β the sweep angle of the A–A' leg. Since this is a kinematic model, we may arbitrarily choose the switchover time to be mid-cycle at $t = T/2$.

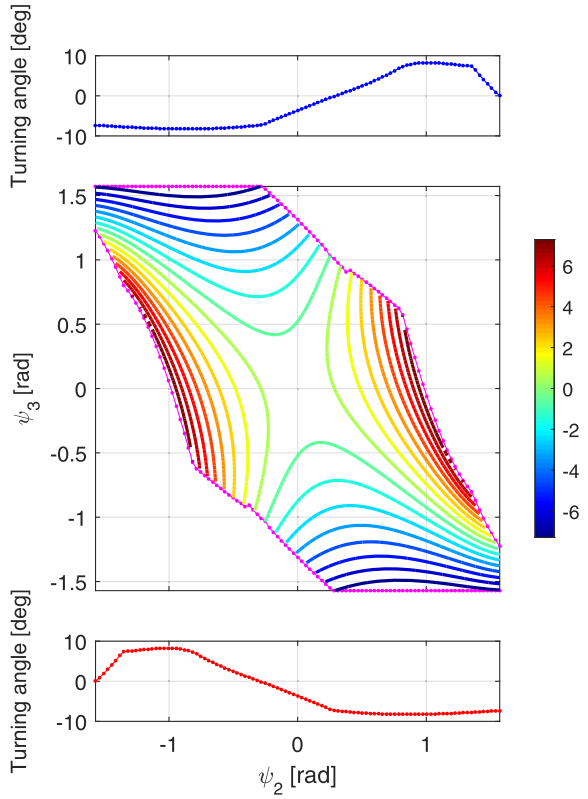

Figure 15. $\beta(T)$ for all non-slip gaits of Mechapod. The overall turn $\beta(T)$ (colored contours, center subplot) after a cycle of non-slip motion for feasible non-slip gaits, and its value on the two boundaries of the feasible range (magenta dots in center; top and bottom graphs), which also show the extremal values.

The use of bootstraps facilitates homoscedasticity of the box-plots we use to represent the results, and allows the spread to be meaningfully compared across groupings. The results show that s reliably governed steering across all 3 robots, and produced statistically indistinguishable outcomes with them. They further show that once the influence of s is removed, neither gait frequency nor substrate friction have a detectable influence on the rate of turning. This suggests a very peculiar physics: one that is geometric by its independence from time parameterization, includes significant slipping, and yet is nearly independent of the magnitude of the friction coefficients that govern this slipping.

To gain further insight into how such a counter-intuitive outcome might appear, we analyzed several slipping metrics of individual legs at different values of the steering parameter s, holding the

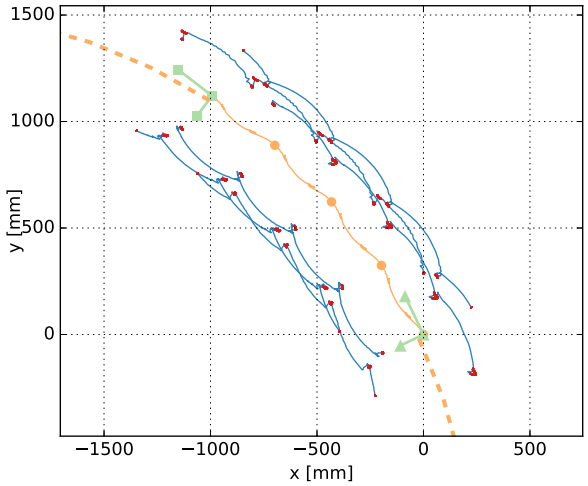

Figure 16. Mechapod maximal predicted turning rate non-slip gait. We plotted the trajectories of the feet (solid hairine blue), and highlighted their positions on the ground (red dots). We also plotted the motion of the body frame (green), indicating start position (green triangles), end position (green squares), position at start of each cycle (yellow circle), position over time (yellow line), and best-fit circular arc (dashed thick yellow line). The robot walked 4 cycles at a frequency of 0.33 Hz. Results show that feet do in fact hardly slip at all. In this trial, Mechapod turns 8.0 deg/cyc and the turning radius is 2692 mm

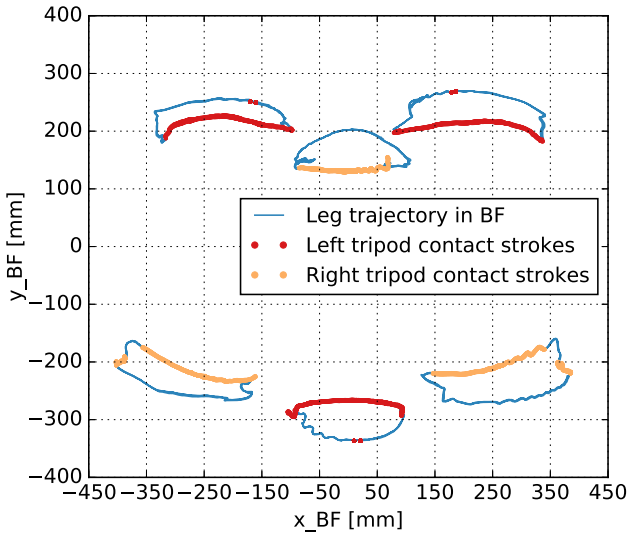

Figure 17. Mechapod body frame foot motions from the trial shown in figure 16. Robot moves to the right. We determined ground contact frames based on the vertical height of the feet from motion tracking. Since the legs are highly elastic, the feet did bounce in and out of contact as shown.

remaining parameters constant. These results are in figure 11, and come from the $f = 0.22$ Hz trials with robot R1.

From figure 11(a) we observe that the slip ratio, which equals total distance slipped divided by total distance traveled, clearly increases with s. The change is expressed mostly in the tangent direction, where legs of the left tripod (FL, MR, HL) are retarded more with higher s, and legs of the right tripod (FR, ML, HR) are advanced. These changes are straight-forward to anticipate from equation (2). The radial direction harbors a surprise: FL and HL respond to changes in s quite strongly and with opposite sign, but their symmetric counter-parts FR and HR do not. This suggests that during left tripod stances with large s, FL moves radially in (right) and HL moves radially out (left), whereas in right tripod stances little to no radial motion is observed.

3.2. Mechapod 2-DoF hexapedal robot

To explore the relationship of slipping and steering with 2-DoF legs, we used the 'Mechapod' robot, a hexapedal robot drived from a previously studied 'centipede robot' [Sastra *et al* 2008, Sastra *et al* 2012]. Centipede attempted to be the first modular robot to exhibit a dyanmic gait with aerial (ballistic) phases using geared-down, conventional servo motors. Mechapod consists of an articulated spine with 7 motor modules, connected to 3 elastic legs that extend side-to-side (see figure 12).

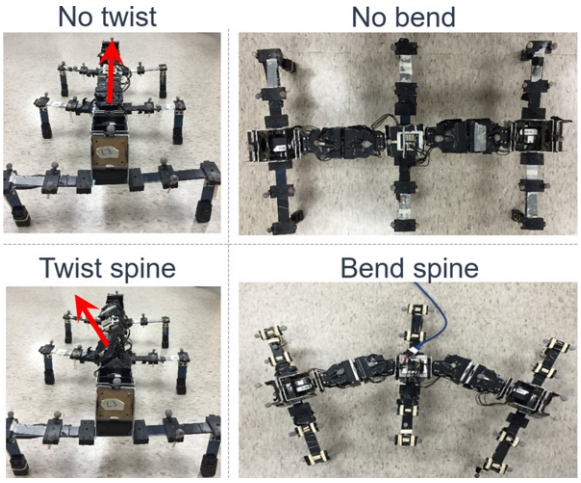

Figure 18. Mechapod neutral position and its modulation for steering. When the Mechapod is moving without turning, its shape oscillates around the shapes shown in the top row. By adding spine twist, the spine leans on average (bottom left); by adding spine bend, the spine is arced on average (bottom right). See supplementary videos for illustrative examples.

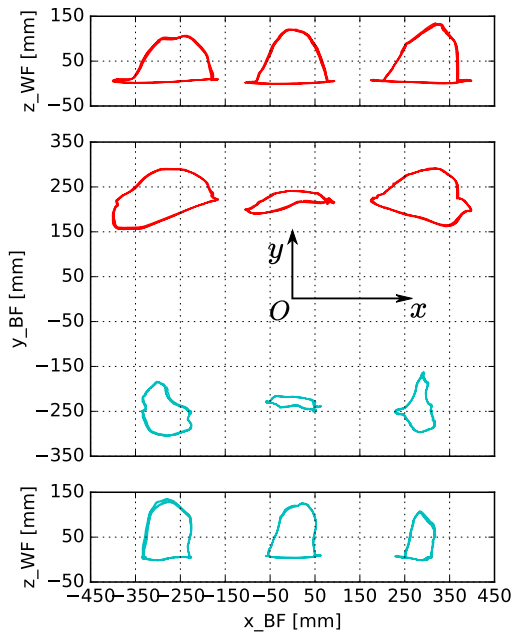

Figure 19. Foot motions in body frame x, y and world z for trial in figure 20. We plotted the motion of the left legs (top subplot, red in middle subplot), and the right legs (bottom subplot, teal in middle subplot). The twist-based steering gait produced shorter ground strokes on the right than on the left, commensurate with a turn to the right.

Defining a body frame for shape-changing robots can be non-trivial [Hatton and Choset 2011]. Following previous work [Sastra *et al* 2012], we associate a body frame with Mechapod by taking the line connecting the center of one end-module ('front') with the center of the opposite end-module ('back') as the X axis, and constraining the center of the middle module to the Y axis. With respect to this body fame, each of the robot's feet can be thought of as under 2-DoF control: one 'yaw' DoF coming from the adjacent Z-axis motor(s) on the spine, and one 'roll' DoF coming from the X-motor to which the leg is attached. The remaining 1-DoF that is unaccounted for allows the spine to roll with respect to the ground without moving the legs.

3.2.1. Mechapod non-slip steering gaits

We considered the problem of introducing steering into the alternating tripod gait used for rapid motion with the Mechapod. When engaging in this gait, the roll motors in the front, middle, and hind modules are typically set to the same fixed angle with alternating signs. Under the assumption that this angle is small, its cosine is nearly constant. This allowed us to plan the motion of the 3D robot in terms of its 2D horizontal projection, which consists of two 4-bar linkages tied together. Each 4-bar has one DoF allowing the robot to move while maintaining non-slip contact with the ground. The idea of embedding such a 4-bar linkage to allow non-slip motion was an insight of the original 'centipede robot' designer (S. Sastra of [Sastra *et al* 2008]; see figure 13).

We construct a periodic 4-bar gait as follows (refer to figure 14). Assuming a cycle with period T, we take $t = 0$ as start of support for one tripod, and $t = T/2$ as switch to support by the other tripod. At time $t = T$, the robot configuration needs to cycle back to the same configuration as that at time $t = 0$ to have a periodic solution, so distances between foot locations must satisfy $|AB(0)| = |AB(T)|$ and $|A'B'(0)| = |A'B'(T)|$. With the non-slip constraint, the supporting legs are pinned to the ground. During the first step ($0 \leqslant t \leqslant T/2$), feet A, B are on the ground; during the second step ($T/2 \leqslant t \leqslant T$), feet A', B' are on the ground. Thus $|AB(0)| = |AB(T/2)|$ and $|A'B'(T/2)| = |A'B'(T)|$; together with the previous equalities, this gives:

$$|AB(0)| = |AB(T/2)| \quad |A'B'(0)| = |A'B'(T/2)| \quad (3)$$

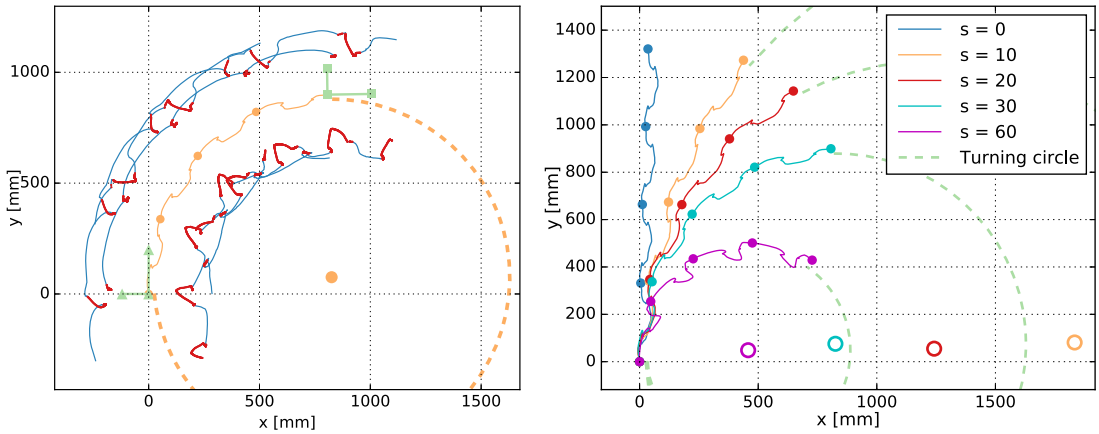

Figure 20. Mechapod motions with $k_{\text{twist}} = 1, k_{\text{bend}} = 0, s = 30°$ (left) and twist gait on low friction surface, for $s = 0, 10, 20, 30, 60(°)$ (right). We plotted the trajectories of the feet (solid hairine blue), and highlighted their positions on the ground (red dots). We also plotted the motion of the body frame (green), indicating start position (green triangles), end position (green squares), position at start of each cycle (yellow circle), position over time (yellow line), and best-fit circular arc (dashed thick yellow line). The robot walked 4 cycles at a frequency of 0.33 Hz and turned 22.3 deg/cyc, for a turning radius of 860 mm. Results show that feet slipped a great deal. For other values of $s = 0, 10, 20, 30, 60(°)$ we plotted (right) location of body frame (solid) with COM after each cycle (solid circles), best fit turning arc (green dashed) and center of rotation (open circle).

Assuming we start a step with $[\beta(0), \psi_2(0), \psi_3(0)]$ at $t = 0$, and by definition $\beta(0) := 0$, the 4-bar structure dictates the distances $|AB|$ and $|A'B'|$ as a function of β, and through $\beta(t)$ as a function of t. The solution of equation (3) thus uniquely selects possible values of $\beta(T/2)$ as an implicit function of the initial $\psi_2(0), \psi_3(0)$. This implies that by exhaustively scanning choices of these initial values we can discover all possible non-slip Mechapod gaits. We performed such an analysis, showing $\beta(T)$ as a result of initial values $\psi_2(0), \psi_3(0)$, also taking into account to forbid poses that would cause self-interference (see figure 15). The maximal turning rate this analysis predicted was 8.09 deg/cyc, given the dimensions of the physical Mechapod.

We tested the maximal non-slip turning gait going forward and back on the robot (total of $N = 34$ trials, $N_s = 136$ strides, $N_f = 6.12 \times 10^4$ frames of data; see one such trial in figure 16). Going forward, the robot averaged 6.7 deg/cyc turning, and going back 9.6 deg/cyc. Thus, on average this gait produced 8.15 deg/cyc of turning while steering—a very close correspondence to the theoretical prediction of 8.09 deg/cyc. The turning angle difference between forward and backward motion comes from the fact that Mechapod is not perfectly symmetric. Examining the foot motions in the robot body frame (see figure 17) shows that right tripod stance trajectories closely follow the concentric arcs expected from the theoretical analysis in figure 4, whereas left tripod stance motions are far less arced. The robot turned strongly to the left in right tripod steps, and then turned a little back to the right in left tripod steps.

We note an additional complication of using this method to produce non-slip steering: to steer we need a parametric family of gaits controlled by a steering parameter $-1 \leqslant s \leqslant 1$ (here ± 1 chosen as limits wlog). This requires being able to solve $\psi_2(t, s)$ and $\psi_3(t, s)$ such that for every value of s we obtain a non-slip motion—thus solving the 4-bar kinematics in real-time. We must then also choose a family of non-slip gaits such that $[\psi_2(0, s), \psi_3(0, s)]$ traces a path from the extremal left turn at $s = -1$, through a no-turning gait at $s = 0$, and finally to e.g. $s = 1$ for the extremal right turn. Ideally, this path should be chosen such that the turn angle is proportional to s. While these additional steps are straightforward to implement, the goal of the current investigation was to compare non-slip steering and steering which employs slipping.

3.2.2. Mechapod steering gaits with slipping

As an alternative to producing a non-slip steering gait, we explored steering the tripod gait with various modulations. The gait we employed was of the form:

$$\begin{aligned} \psi_1 = -\psi_4 = \psi_7 &:= A_{\text{roll}} \sin(\varphi) \\ \psi_2 = -\psi_6 &:= A_{\text{yaw1}} \cos(\varphi) \\ \psi_3 = -\psi_5 &:= A_{\text{yaw2}} \cos(\varphi) \end{aligned} \tag{4}$$

We then introduced two types of modulation 'spine twist' where all roll motors were given a constant offset to the same side causing the robot to lean to one side, and 'spine bend' where all yaw motors were given a constant offset to the same side causing the neutral shape of the spine to be bent along an arc (see figure 18). These modulations were introduced as follows: the updated motor angles $\psi_i'(\varphi, s)$ were given by $\psi_i'(\varphi, s) = k_{\text{twist}} s + \psi_i(\varphi)$ for $i \in \{1, 4, 7\}$, and $\psi_i'(\varphi, s) = k_{\text{bend}} s + \psi_i(\varphi)$ for $i \in \{2, 3, 5, 6\}$. This allowed us to introduce various combinations of bending and twisting, and test their efficacy at producing steering.

Table 2. Steering and slipping results for trials in figure 20. Slip in this table are averaged by leg then by gait cycle.

s (°)	Deg/cyc	R (mm)	Slip (mm/cyc)	Slip ratio (%)
10	8.1	1802	129	26.5
20	14.2	1312	133	26.9
30	22.3	860	138	29.2
60	32.8	437	186	36.2

As expected, making either k_{twist} or k_{bend} nonzero produced reliable steering gaits. We presented various combinations of bending and twisting in [Zhao and Revzen 2016, Zhao *et al* 2015]. The effect of bending ($k_{\text{bend}} > 0$) followed intuition quite well—when the spine was bent, the robot turned around a center of rotation on the inside of the average arc of the spine (although not around the center of the spine's arc). Twisting ($k_{\text{twist}} > 0$) produced even better steering performance, where leaning to the left caused the robot to steer right; the mechanism of this steering result remains somewhat unclear.

We investigated the twist-based steering gait for the Mechapod using similar analyses to those used for BigAnt (see figures 19 and 20). Table 2 gives the corresponding quantitative steering performance and slipping metrics.

The largst twist steering parameter we used was $s = 60°$. With this value, the Mechapod turned approximately 33 deg/cyc, about $\times 4$ better than the best non-slip steering performance. This turning rate is far better than BigAnt and the robots investigated by Zarrouk *et al* [Zarrouk *et al* 2015]. It is also worth noting the slip ratios at approximately 36%, almost double that of cockroaches.

4. Conclusion and discussion

Multi-legged robots are not in common use, despite their inherent stability and the mechanical robustness that can be achieved with three or more legs contacting the ground at once. Two factors that might be limiting their deployment are the mechanical complexity of building many multi-DoF legs, and the difficulty in understanding and planning for the multi-contact regimes that arise when these robot morphologies are employed. The first factor can be addressed by using legs with only 1 or 2 DoF each, and this category of robots was the topic of our study here. We presented two hexapedal robots with 6 and 7 motors, respectively. The 6 motor BigAnt has 1-DoF legs; the 7 motor Mechapod has, for all practical purposes, 2-DoF legs.

Under the assumption that we wish, at minimum, to steer the robots on a horizontal plane, we showed how these appealing low-complexity morphologies raise unique problems related to multi-legged locomotion in general, and underactuation in particular. We showed that for the robots in question, there exist natural ways to produce steering, and illuminated some of the special relationship between bilateral symmetry and steering. We showed that the best steering gaits we produced do not obey the non-slip contact conditions robot designers usually employ in planning. For the BigAnt, non-slip conditions would have precluded turning altogether. For the Mechapod, non-slip steering gaits do exist, but under-perform ad hoc steering gaits we tried by a factor of $\times 4$.

The careful examination of mechanism of turning in both BigAnt and Mechapod lead to some surprising results. The relationship between Mechapod shape modulation and steering outcome proved difficult to elucidate. More interestingly, BigAnt motions proved to be independent of speed and friction coefficient, suggesting that a geometric theory similar to that which governs slithering snake robots [Gong *et al* 2016] might be applicable. An initial foray into how the viscous-friction-like relationships of geometric mechanics arise from simple Coulomb friction models can be found in our recent publication Wu *et al* [Wu *et al* 2019].

Taken together this evidence suggests that design of multi-legged robot gaits raises some new issues related to phase, but effective solutions for steering are not hard to find, and do not require the full complexity of 3 or more DoF per leg. The key issue is that steering gaits, and by extension, other high-performance maneuvers, must assume that slipping will invariably take place, and be an integral part of the planned motion. This does not, however, imply that multi-legged maneuvers require knowledge of friction coefficients or planning in the full phase space, as some might have assumed. At least for our robots, it seems that some kind of geometric mechanics theory is lurking just around the corner, and with it we will be able to reap the benefits of simple and robust multi-legged robot morphologies.

5. Future work

One obvious important direction of future investigation is developing and validating physics codes for multi-legged locomotion which can handle the persistent slipping that we have discovered to be necessary for effectively steering our robots. Besides building better models that include slipping, another interesting approach is to explore the potential of non-slip gaits with low-DoF legs. We have shown that Mechapod can have non-slip steering gaits with only 7 motors; perhaps other low DoF per leg designs can be produced which have better steering performance. Yet another important direction to explore is the high-speed limit: how do the approaches we studied here extend as robots move faster, inertia plays a larger role, and power rather than torque limits the motors?

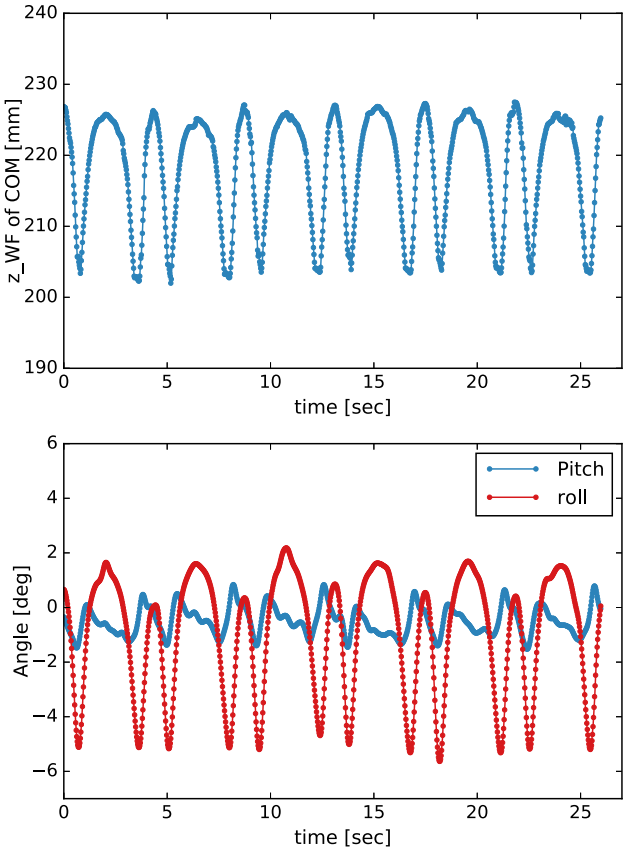

Figure A1. World frame z motion of BigAnt COM(top), pitch and roll (bottom) with $s = 0.75f = 0.22$Hz

Acknowledgments

Work on this project was funded by ARO W911NF-14-1-0573, W911NF-17-1-0243, and W911NF-17-1-0306, as well as NSF CMMI 1825918.

Appendix A. Pitch and roll data

Here we provide some examples (world frame z motion of COM figure A1; pitch and roll angle figure A1) of BigAnt, demonstrating its stability.

ORCID iDs

Dan Zhao https://orcid.org/0000-0003-0095-0818
Shai Revzen https://orcid.org/0000-0002-2989-0356

References

Bloch A M, Marsden J E and Zenkov D V 2005 Nonholonomic dynamics *Not. AMS* **52** 320–9

Duan X, Chen W, Yu S and Liu J 2009 Tripod gaits planning and kinematics analysis of a hexapod robot *2009 IEEE Int. Conf. on Control and Automation* (IEEE) pp 1850–5

Fitzner I, Sun Y, Sachdeva V and Revzen S 2017 Rapidly prototyping robots: using plates and reinforced flexures *IEEE Robot. Autom. Mag.* **24** 41–7

Franklin R, Bell W J and Jander R 1981 Rotational locomotion by the cockroach *Blattella germanica J. Insect Physiol.* **27** 249–55

Galloway K C, Haynes G C, Ilhan B D, Johnson A M, Ryan K, Lynch G A, Plotnick B N, White M and D E K 2010 X-rhex: Highly Mobile Hexapedal Robot for Sensorimotor Tasks *Technical Report* University of Pennsylvania

Gong C, Travers M J, Astley H C, Li L, Mendelson J R, Goldman D I and Choset H 2016 Kinematic gait synthesis for snake robots *Int. J. Robot. Res.* **35** 100–13

Haldane D W and Ronald S F 2014 Roll oscillation modulated turning in dynamic millirobots *2014 IEEE Int. Conf. on Robotics and Automation (ICRA)* (IEEE) pp 4569–75

Hatton R L and Choset H 2011 Geometric motion planning: the local connection, Stokes' theorem, and the importance of coordinate choice *Int. J. Robot. Res.* **30** 988–1014

Jindrich D L and Full R J 1999 Many-legged maneuverability: dynamics of turning in hexapods *J. Exp. Biol.* **202** 1603–23

Johnson A M 2013 Robot Parkour: The Ground Reaction Complex & Dynamic Transitions *Dynamic Walking*

Kim S, Clark J E and Cutkosky M R 2006 iSprawl: design and tuning for high-speed autonomous open-loop running *Int. J. Robot. Res.* **25** 903–12

Kvalheim M, Bittner B and Revzen S 2019 Gait modeling and optimization for the perturbed Stokes regime *Nonlinear Dyn.* **97** 2249–70

Marsden J E and Ostrowski J 1998 Symmetries in Motion: Geometric Foundations of Motion Control *Motion, Control, and Geometry: Proc. of a Symposium*

McClung A J 2006 Techniques for dynamic maneuvering of hexapedal legged robots *PhD Thesis* Stanford University

Miller D, Fitzner I, Fuller S B and Revzen S 2015 Focused modularity: rapid iteration of design and fabrication of a meter-scale hexapedal robot *Assistive Robotics: Proc. of the 18th Int. Conf. on CLAWAR 2015* (Singapore: World Scientific) pp 430–8

Proctor J and Holmes P 2008 Steering by transient destabilization in piecewise-holonomic models of legged locomotion *Regul. Chaotic Dyn.* **13** 267–82

Pullin A O, Kohut N J, Zarrouk D and Ronald S F 2012 Dynamic turning of 13 cm robot comparing tail and differential drive

2012 IEEE Int. Conf. on Robotics and Automation (IEEE) pp 5086–93

Revzen S, Koditschek D E and Full R J 2008 *Progress in Motor Control—A Multidisciplinary Perspective, Chapter towards Testable Neuromechanical Control Architectures for Running* (Berlin: Springer Science & Business Media) pp 25–56

Shekhar Roy S and Kumar Pratihar D 2014 Kinematics, dynamics and power consumption analyses for turning motion of a six-legged robot *J. Intell. Robot. Syst.* **74** 663–88

Sachdeva V, Zhao D and Revzen S 2018 Cockroaches always slip a lot *Integr. Comp. Biol.* **58** E412

Saranli U, Buehler M and Koditschek D E 2001 Rhex: a simple and highly mobile hexapod robot *Int. J. Robot. Res.* **20** 616–31

Sastra J, Revzen S and Yim M 2012 Softer legs allow a modular hexapod to run faster *Adaptive Mobile Robotics* (Singapore: World Scientific) pp 507–10

Sastra J, Bernal-Heredia W G, Clark J and Yim M 2008 A biologically-inspired dynamic legged locomotion with a modular reconfigurable robot *Proc. of DSCC ASME Dynamic Systems and Control Conf.* pp 1467–74

Schmitt J and Holmes P 2000 Mechanical models for insect locomotion: dynamics and stability in the horizontal plane I. Theory *Biol. Cybern.* **83** 501–15

Seipel J E, Holmes P J and Full R J 2004 Dynamics and stability of insect locomotion: a hexapedal model for horizontal plane motions *Biol. Cybern.* **91** 76–90

Simon W, Reeve M A, Haynes G C, Revzen S, Koditschek D E and Spence A J 2017 Longitudinal quasi-static stability predicts changes in dog gait on rough terrain *J. Exp. Biol.* **220** 1864–74

Wu Z, Zhao D and Revzen S 2019 Coulomb friction crawling model yields linear force–velocity profile *J. Appl. Mech.* **86** 054501

Zarrouk D and Ronald S F 2015 Controlled in-plane locomotion of a hexapod using a single actuator *IEEE Trans. Robot.* **31** 157–67

Zarrouk D, Haldane D W and Ronald S F 2015 Dynamic legged locomotion for palm-size robots *Proc. SPIE* **9467** 94671S

Zhao D and Revzen S 2016 Slipping helps steering in a multilegged robot *Dynamic Walking*

Zhao D, Schaffer C M and Revzen S 2015 Steering hexapedal robots *Workshop on Miniature Legged Robots, Conf. on Robotics Science and Systems* (13-17 July 2015 Sapienza University of Rome Rome, Italy)

Zolotov V, Frantsevich L and Falk E M 1975 The kinematics of phototactic turns in the honeybee *J. Comp. Physiol.* **97** 339–53